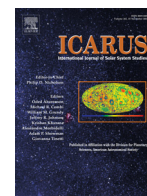




Contents lists available at ScienceDirect

Icarus

journal homepage: www.elsevier.com/locate/icarus

Compressive strength and elastic modulus at Agilkia on comet 67P/Churyumov-Gerasimenko derived from the SESAME/CASSE touchdown signals

Diedrich Möhlmann^{a,1}, Klaus J. Seidensticker^a, Hans-Herbert Fischer^b, Claudia Faber^a, Alberto Flandes^c, Martin Knapmeyer^a, Harald Krüger^d, Reinhard Roll^d, Frank Scholten^a, Klaus Thiel^e, Walter Arnold^{f,g,*}

^aDLR Institute of Planetary Research, Rutherfordstr. 2, 12489 Berlin, Germany

^bDLR Microgravity User Support Center, Linder Höhe, 51147 Köln, Germany

^cInstituto de Geofísica, Universidad Nacional Autónoma de México, Coyoacán 04510, Mexico City, Mexico

^dMax Planck Institute for Solar System Research, Justus-von-Liebig-Weg 3, 37077 Göttingen, Germany

^eNuclear Chemistry Department, University of Cologne, Zùlpicher Str. 45, 50674 Köln, Germany

^fSaarland University, Department of Materials Science and Technology, Campus D 2.2, 66123 Saarbrücken, Germany

^gI. Physikalisches Institut, Georg-August University, Friedrich-Hund-Platz 1, 37077 Göttingen, Germany

ARTICLE INFO

Article history:

Received 4 February 2017

Revised 22 September 2017

Accepted 28 September 2017

Available online xxx

Keywords:

Comet surface material

Compression strength

Elasticity

ABSTRACT

We report an analysis of the Comet Acoustic Surface Sounding Experiment (CASSE) acceleration signals at Philae's first touchdown site Agilkia on comet 67P/Churyumov-Gerasimenko. The signals yield the forces in the contact zone foot-sole and comet surface, and from these forces a compression strength of approximately 10 kPa can be derived. The sole's contact-resonances provide an elastic modulus of the order of 10 MPa. Our results are partially based on calibration experiments, which are described in the appendix of the current paper. Relations known in material science, linking porosity to elasticity and fracture energy, allow one to check the interdependence between compression strength and elasticity.

© 2017 The Authors. Published by Elsevier Inc.

This is an open access article under the CC BY-NC-ND license.

(<http://creativecommons.org/licenses/by-nc-nd/4.0/>)

1. Introduction

Elasticity in a highly porous material is primarily determined by the elasticity of its constituents and its porosity (Pabst et al., 2006). Its mechanical strength is linked to a number of properties such as the adhesion forces between the constituents or particulates of the material, its porosity, the distribution and orientation of cracks, inclusions, and cavities. The elasticity and the mechanical strength of any material and hence also of a cometary surface material cannot be measured remotely, because elasticity and plastic deformation can only be probed by forces and by measuring the ensuing deformations in situ. The landing of Philae on comet 67P/Churyumov-Gerasimenko at Agilkia provides direct access to determine surface elasticity and plastic deformation by analyzing the data obtained by accelerometers mounted on the bot-

tom of the Philae lander soles. We use the accelerometer data to derive the forces, that acted in the contact zone between the sole and the comet surface at Agilkia corroborating the analysis of the bouncing dynamics which allowed a first estimate of the comet surface compression strength of some kPa at the ~10 cm to 1 m scale (Biele et al., 2015). A detailed finite element multi-body simulation analysis code from SIMPACK (Version 9.5.1) as well as analytical estimates based on the lander internal dynamics led to similar values for the compression strength (Roll and Witte, 2016; Roll et al., 2016).

First, a brief account of the landing events is given according to Biele et al. (2015). On November 12th, 2014, the lander Philae was separated from the Rosetta orbiter. The separation of Philae occurred with a relative velocity of $\Delta v = 0.1876$ m/s at about 20.5 km altitude at 08:35:00 UTC. After 6:59:04 h of ballistic descent, which was tracked by the CONSERT (Comet Nucleus Sounding Experiment by Radiowave Transmission) instrument (Kofman et al., 2015), Philae landed at 15:34:03.98 ± 0.10 s UTC (first touchdown TD1) at Agilkia on comet 67P. The time refers to the trigger signal at the vertical axis of the +Y-foot CASSE accelerometer. The

* Corresponding author at: Saarland University, Department of Materials Science and Technology, Campus D 2.2, 66123 Saarbrücken, Germany.

E-mail address: w.arnold@mx.uni-saarland.de (W. Arnold).

¹ Deceased.

<https://doi.org/10.1016/j.icarus.2017.09.038>

0019-1035/© 2017 The Authors. Published by Elsevier Inc. This is an open access article under the CC BY-NC-ND license. (<http://creativecommons.org/licenses/by-nc-nd/4.0/>)

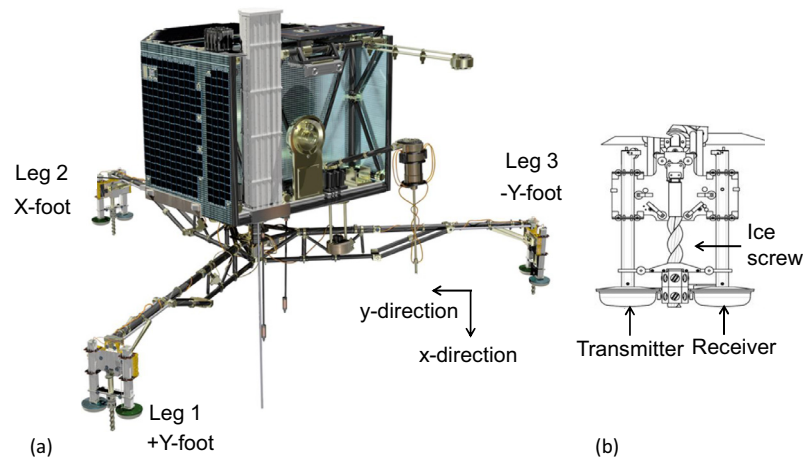


Fig. 1. (a) Definition of the Philae lander coordinate system (X, Y, Z) and the accelerometer x-, y-, and z-coordinates. Leg 1 holds the +Y-foot, Leg 2 holds the +X-foot, and Leg 3 holds the -Y-foot. The coordinate system of each accelerometer is defined locally. The x-directions of all accelerometers in each of the right foot soles (seen from the outside) point downward. The y-direction is parallel to the legs of the landing gear pointing inward, whereas the z-direction is perpendicular to the x- and y-directions forming a right-handed coordinate system; (b) Detail of one double foot: The left sole houses the CASSE transmitter whereas the right sole houses a B&K tri-axial accelerometer as receiver. The “ice screw” served for fixation of the lander on the comet soil (color online).

descent trajectory was perpendicular to the surface of the landing site. Indeed, the reconstruction showed that before touchdown the angle between the incoming velocity vector and the surface normal was 0.9° . However, due to a local slope of the terrain, the incoming velocity was $11.5 \pm 1^\circ$ away from the local normal. Philae arrived with a velocity vector mainly parallel to the lander z-axis, but left with a lateral velocity to the South-East of magnitude 32.5 cm/s . The touchdown speed relative to the comet surface was 1.012 m/s (Roll and Witte, 2016).

At touchdown the central damping tube of Philae’s landing gear was pushed in against the main lander head, generating the touchdown signal which occurred at $15:34:06.471 \pm 1 \text{ s}$ UTC (Biele et al., 2015) with a few seconds delay to the first CASSE signal. The stroke length of the damper was $42.6 \pm 0.1 \text{ mm}$ out of a full length of $\sim 170 \text{ mm}$. The landing gear damper did not move after leaving Agilkia, i.e. the component of force in lander’s z direction during further touchdowns must have been $< 30 \text{ N}$, due to static friction in the mechanism. Because the anchor harpoons did not fire upon touchdown and the hold-down thrust of the cold gas system did not work, the lander bounced several times until it came to rest after about 2 h of ballistic flight. Further details of the landing events at Agilkia can be found elsewhere (Roll and Witte, 2016).

This paper is organized in the following way: First, a short introduction to contact mechanics is given followed by the description of the CASSE signals. We then analyze the signals by treating the foot soles as contact oscillators. The surface compression strength and elastic modulus derived is compared to data obtained from scaling laws known in materials science for very porous materials. Eventually the data are compared to strength results obtained from other experiments of the Rosetta mission and to the data obtained by the KOSI (“Kometsimulation”) experiments.

2. Comet acoustic surface sounding experiment (CASSE)

A double foot is fixed to each of the landing gear legs. One sole of the foot contains an accelerometer and the other a piezoelectric transmitter. Viewed from the outside, the transmitter is in the left sole, whereas the accelerometer is in the right sole (for the definition of Philae’s axes, see Fig. 1). The original operation principle of CASSE was to insonify the comet at frequencies from 0.5 kHz to 1 kHz by the soles containing the transmitter and to receive the signals by the soles in which Bruel & Kjaer (B&K) triaxial accelerometers were mounted. Details of this set-up are described elsewhere (Seidensticker et al., 2007).

Additionally, CASSE was also used to measure the accelerations of the landing shock and the sole’s contact-resonances when the feet touched ground the first time on comet 67P at Agilkia. The strength of the landing shock or the force acting between Philae’s landing gear and the comet soil is determined on the one hand by the compliance of the material encountered at the landing location and, on the other hand, by the compliance of that part of the landing gear which touches the surface. Besides the absolute value of the force of the landing shock, the forced resonances of the soles of the feet can be used to obtain information on the local elastic modulus E and the compression strength σ_c of the comet soil. These principles and mode of operation have been discussed in an earlier paper describing the evaluation of the landing tests at the Landing & Mobility Test Facility (LAMA Tests) (Faber et al., 2015).

3. Philae’s landing and contact mechanics

The elastic, anelastic, and plastic interactions between the landing soles and the comet body are determined by the contact stiffness k^* (inverse of the compliance):

$$k^* = 2E_r^*(A_c/\pi)^{0.5}, \quad (1)$$

where E_r^* is the effective storage modulus of the contacting materials, here the comet soil and that part of the landing gear which touches the surface, and A_c is the contact area. The quantity E_r^* contains the elastic moduli of both contacting partners (Johnson, 1985), here the comet soil E_c and the foot soles E_{sh} , and their Poisson ratios ν_c and ν_{sh} :

$$1/E_r^* = 1/E_{r,c} + 1/E_{r,sh} = (1 - \nu_c^2)/E_c + (1 - \nu_{sh}^2)/E_{sh}, \quad (2)$$

where $E_{r,c}$ and $E_{r,sh}$ are the reduced elastic moduli of the comet soil and the foot sole, respectively. Eq. (2) is valid for homogeneous, isotropic and volumetric materials. The foot sole, however, is a thin shell structure. We will accommodate Eq. (2) to this fact later on when required. The parameter E_r^* reflects the fact that displacements occur in both contacting materials. Eq. (1) is a very general relation that applies to any axisymmetric indenter. It is not limited to a specific simple geometry. Although originally derived for elastic contacts only, it has subsequently been shown to apply equally well to elastic-plastic contacts. Small perturbations from an axisymmetric geometry in the contacting materials do not effect k^* either. It is also unaffected by pile-up of the material and

sink-in of the indenter (Oliver and Pharr, 2004). In case of a sphere against a flat surface, the contact stiffness is given by

$$k^* = 2a_c E_r^* \quad (3)$$

where a_c is the contact radius. In case of viscous damping or plastic deformation, k^* becomes a complex quantity $k^* = k_r + ik_i$ (Yuya et al., 2008) with $k_i = 2E_i^*(A_c/\pi)^{0.5}$ where E_i^* is the corresponding loss modulus and $k_r = 2E_r^*(A_c/\pi)^{0.5}$ is the real part of the contact stiffness (Eq. (1)). The relation of contact stiffness to material properties has been exploited in particular in nanoscale measurements, i.e. for contact radii less than 100 nm both in nanoindentation experiments (Landman et al., 1990; Oliver and Pharr, 2004) and in atomic force microscopy (Arnold, 2012). In our case, as it will become clear, the contact radius a_c can be as large as the geometrical radius of the sole, i.e. $r = 5$ cm.

In order to understand the occurrence of contact resonances in Philae's sole, let us consider at the basic behavior of a contact-oscillator. The angular contact-resonance frequency ω_{ct} of two freely supported bodies of masses m_1 and m_2 can be written as (Johnson, 1985):

$$\omega_{ct}^2 = k^* \times \frac{m_1 + m_2}{m_1 m_2} \quad (4)$$

The masses $m_{1,2}$ are effective masses and depend on the geometry of the oscillator and on the excitation frequency. In particular Philae's soles are mass-distributed oscillators. Therefore, dispersion of the resonance frequency versus contact stiffness or reduced elastic modulus of the contacting partners is to be expected. If there is friction in the contact volume or in any other part of the contact oscillator, $k^* = k_r + ik_i$ becomes complex. This entails the complex reduced modulus mentioned above.

The basic physics of contact vibrations, in particular the behavior at large amplitudes or static loads are discussed in Nayak (1972). Further engineering applications of the contact-resonance technique are discussed in Lange (1994). In atomic force acoustic microscopy the cantilever contact-resonances led to a new mode of operation (Arnold, 2012; Marinello et al., 2013).

During the development and qualification of CASSE, which is part of the Surface Electric Sounding and Acoustic Monitoring Experiment (SESAME), eigenmodes and eigenfrequencies of the soles were characterized. A detailed discussion of the results obtained can be found elsewhere (Arnold et al., 2004; Schieke, 2004). A flight spare sole with mounted accelerometer showed resonance frequencies of approx. 600 Hz and 650 Hz at room temperature (Krause, 2007). The double resonance may be caused by the mounting of the accelerometer relative to the orientation of the glass-fiber fabric of the composite material (GFC = glass-fiber composite) the sole is made of, lifting the degeneracy of the first eigenmode of the sole due to the elastic anisotropy of the GFC (the mass-distribution of the accelerometer is not axially symmetric). This is typical for geometrical oscillators that are not completely symmetric, and similar phenomena were observed for the sole's higher eigenmodes (Arnold et al., 2004; Schieke, 2004). The double resonances were also observed with a different flight spare sole used for calibration purposes, as reported in the Appendix A5. As said above, the possibility to exploit the contact-resonances was evaluated by landing tests at the Landing & Mobility Test Facility (LAMA Tests) (Faber et al., 2015). It is the compression strength σ_c and the reduced modulus $E_{r,c}$ of the comet soil, that we want to extract from the landing shock and the contact-resonances of the Philae's lander gear's soles, respectively.

4. CASSE signals recorded at Agilkia

We discuss first the signals recorded by the CASSE accelerometers at Agilkia. The B&K accelerometers were mounted such that

the x-direction points perpendicular to the sole surface and hence into the comet soil, the y-direction parallel to the corresponding leg into the lander body, and the z-direction perpendicular to the x- and y-direction, forming a right-handed coordinate system, see Fig. 1. The designations of the feet can be seen in Fig. 1 as well.

The accelerometer signals in x-direction of the three feet and their Fourier transforms are shown in Figs. 2–4. The origin of the time axes correspond to 15.34:03.78 ± 0.1 s UTC, see Biele et al. (2015). From the appearance and the amplitude of the signals (Figs. 2a–4a) it becomes clear that the +Y-foot or leg 1 encountered the comet surface in a different way from that of the +X-foot and the –Y-foot. In order to obtain a first overview, we can see that the +Y-foot underwent negative (upward movement) and positive amplitudes (downward movement) of up to ±140 m/s² (when the digitizer saturated) whereas the +X-foot and the –Y-foot experienced values of maximal accelerations in x-direction up to ±40 m/s². Also the Fourier spectra are quite distinct. Additionally, all three feet show low-frequency signals below 300 Hz, there are frequency groups above noise at 0.67 kHz and at 1.3 kHz for the +Y foot (Fig. 2b), whereas for the +X-foot (Fig. 3b) and the –Y-foot (Fig. 4b) there are two groups of frequencies above the noise at 1–1.2 kHz. The fact that both signs occur in these signals means that the soles of the Philae feet, which house the accelerometer, underwent oscillations when encountering the comet surface. These oscillations are analyzed in the following sections. The CASSE signals in all three feet in the y- and z-direction are discussed elsewhere (Seidensticker et al., in preparation).

5. Features of the CASSE signals recorded at Agilkia

Before we discuss the details of the various signals, let us discuss how Philae encountered the comet surface (Biele et al., 2015). In Section 1, a first description of the landing events has been given. In addition, OSIRIS Narrow Angle Camera (NAC) images taken from the Rosetta orbiter were used together with ROLIS (Rosetta Lander Imaging System) descent images in order to determine the actual landing coordinates and attitude at Philae's first landing site, Agilkia (Fig. 5). Altitude, attitude with respect to the surface, and the rotational state were derived independently from this analysis. The motion of the lander close to the surface of 67P comprises, besides the vertical descent with a velocity of $v \approx 1$ m/s, also a counter-clockwise rotation around the main axis of the lander in top view with an angular frequency of $\omega \approx 1.26 \times 10^{-2} \text{ s}^{-1}$ (0.72°/s) (Biele et al., 2015). Because of the strong signals recorded by the sole's accelerometer mounted in the +Y-foot, it is tempting to postulate that the +Y-leg hit the largest boulder with its foot soles or with a strut of the leg as seen in Fig. 5. Possible encounters are depicted schematically in Fig. 6. In view of the uncertainty in spatial (±10 cm) and angular positions (±1°) of the Philae legs relative to the surface, let us begin with the hypothesis that the boulder was hit several times by various parts of the landing gear's leg 1 with the attached +Y-foot with its sole. We will discuss whether this hypothesis is in agreement with observations.

Philae's first contact with the nucleus of 67P at Agilkia was a short "touch" of the +Y-foot, see signals at $t = 160 - 230$ ms (Fig. 2a). The signal strengths of approx. ±10 m/s² are comparatively weak in view of the later values at $t > 450$ ms. The forces acting on the soles initiated momenta influencing the further movements of Philae by tilt rotation and nutation in a rather complex way (Roll and Witte, 2016). A detailed account of this signal as well as the time-sequence of the touchdown signals of the three feet of Philae will be discussed elsewhere (Seidensticker et al., in preparation).

At $t = 437$ ms, with a delay of more than 260 ms from this first signal, strong signals set in for the +Y-foot (Fig. 2a). The onset of

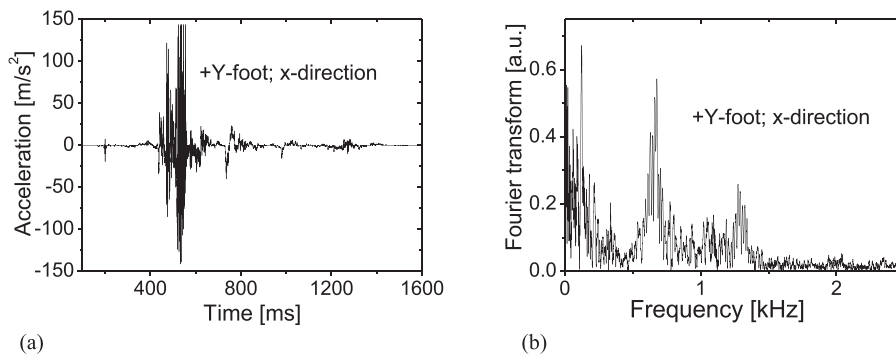


Fig. 2. (a) Acceleration data and (b) its frequency spectrum in x-direction for the +Y-foot.

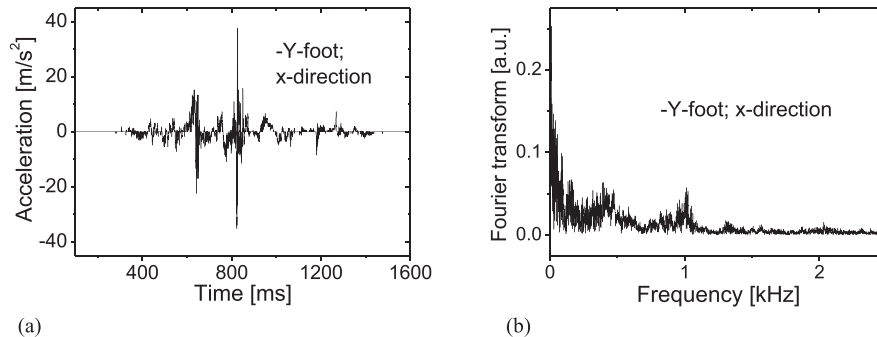


Fig. 3. (a) Acceleration data and (b) its frequency spectrum in x-direction for the -Y-foot.

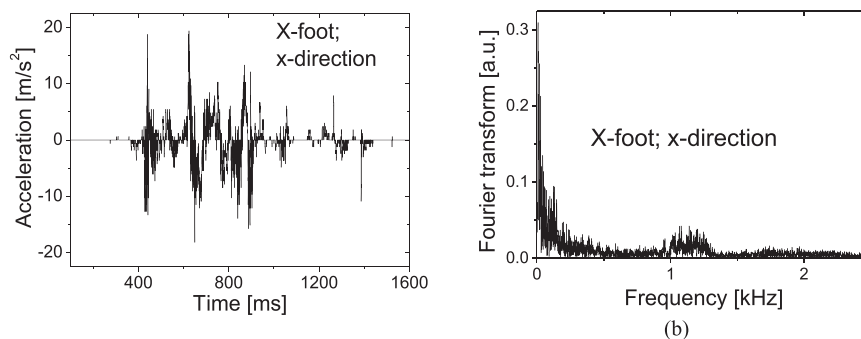


Fig. 4. (a) Acceleration data and (b) its frequency spectrum in x-direction for the +X-foot.

these signals is seen in the y- and z-directions of the accelerometers within 1 ms, i.e. almost simultaneously. Almost at the same time, signals in the +X-foot set in (Fig. 4a), whereas the main signals in the -Y-foot are further delayed by about 200 ms (Fig. 3a).

As can be seen from Figs. 2a to 4a, the signals appear in distinct groups. We first analyze the various parts of the signals in time, amplitude, and spectral components. Although the Fourier transforms of these signals, Figs. 2b–4b, seem to indicate that there are continuous bands of frequencies, this is not the case. If one examines the time series piecewise around the signal groups by counting the oscillations maxima and by short time Fourier transformation (STFT), much narrower frequency peaks become visible which are listed in Tables 1–3. In these tables, the maximal acceleration values in the time windows are given, as well as the dominant frequency peaks.

The spectral components contain dominantly frequencies at 1.3 kHz, 1.1 kHz, 670 Hz, 400 Hz and 300 Hz and an almost continuous spectrum of signals below 300 Hz. These frequencies have bandwidths of the order of 50–100 Hz. If this bandwidth is ascribed to a damping mechanism, the Q-value would be $Q = \omega / \Delta\omega \approx 20 - 10$ which indeed corresponds roughly to the

value measured with a spare sole (see Appendix A5). One has to be careful, however; it might also be due to a distribution of resonance frequencies caused by varying elastic boundary conditions when the sole touches the surface, which entails that there are inhomogeneously broadened resonance-curves.

We propose that these groups reflect individual contacts with the comet surface due to the motion of the lander, the induced oscillations of the landing leg, and the local terrain, in particular the multi-asperity contacts of the lander soles with pebbles of a size distribution down to cm (Mottola et al., 2015). Some of the signals seen in the +X-foot and the -Y-foot may stem from the oscillatory excitation of the whole lander structure by the strong signal from the +Y-foot.

The total stiffness k_t of the spring arrangement, representing one leg of the landing gear, without taking into account the Coulomb friction damping in the ice screws (see Figs. 1b and 8), is given by

$$\frac{1}{k_t} = \frac{1}{k^*} + \frac{1}{k_{sh}} + \frac{1}{k_{LG}} + \frac{1}{i\omega\gamma_D} \quad (5)$$

Here, k^* is the contact stiffness of the sole-comet surface contact, $k_{LG} = 13.3 \text{ kN/m}$ is the stiffness of one leg of the landing gear,

Table 1

Features of the signals of the +Y-foot; x-direction: Amplitudes, main frequency components determined by the time differences in signal maxima and/or by short time Fourier transforms (STFT).

Time interval (s)	Amplitude (m/s ²)	Frequencies (kHz)	Frequencies STFT (kHz)
0.15–0.25	+18/–12	0.38/1.2	0.35/1.2/
0.43–0.47	±32	1.1	0.7/1.1/1.2
0.47–0.5	+120/–81	0.68	0.68/1.3
0.5–0.6	+140/–140; Clipped signals	0.67/1.05/1.3	0.67/1.05/1.3
0.6–0.9	+25/–33	0.43/1.1	0.35/0.75/1.1
0.9–1.6	+7/–15	0.335/1.1	0.34/1.1

Table 2

Features of the signals of the –Y-foot; x-direction: Amplitudes, main frequency components determined by the time differences in signal maxima and by short time Fourier transforms (STFT).

Time interval (s)	Amplitude (m/s ²)	Frequencies (kHz)	Frequencies STFT (kHz)
0.3–0.6	5/–5	0.38/1.03	0.34/1.02
0.6–0.8	23/–32	0.35/1.05	0.35/1.01
0.8–1.0	40/–30	0.47/0.98	0.42/0.96
1.0–1.6	8/–7	0.41/1.1	0.43/1.1

Table 3

Features of the signals of the +X-foot; x-direction: amplitudes, main frequency components determined by the time differences in signal maxima and by short time Fourier transforms (STFT).

Time interval (s)	Amplitude (m/s ²)	Frequencies (kHz)	Frequencies STFT (kHz)
0.3–0.6	20/–12	0.38/1.1	0.38/1.16
0.6–0.75	18/–18	1.1	1.1/1.2
0.75–1.0	11/–15	1.1	1.1/1.2
1.0–1.6	8/–10	1.05	0.68/1.05

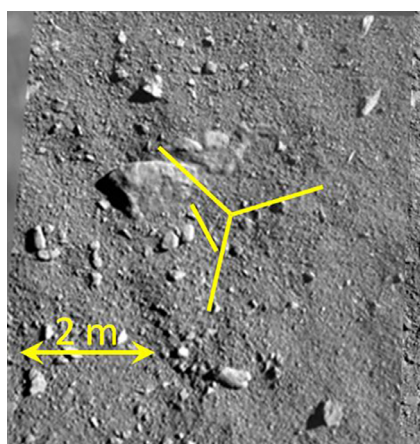


Fig. 5. Extrapolated lander position and orientation during Philae's first contact with the comet at the site Agilkia. The lander legs are to scale and superimposed on merged and rectified ROLIS images. North is up. The thin yellow line indicates the lander balcony edge. The landing gear was rotated during decent by 11°. The +Y leg hits the edge of the boulder seen in the center of the image. The resolution of the ROLIS image is 2 cm/pxl (full-resolution) and the positional uncertainty of Philae relative to the surface is ±10 cm. This figure is an updated version of the one shown in Biele et al. (2015) (color online).

and $k_{sh} = 270$ kN/m is the stiffness of the sole (see Appendix A3, Fig. A3.2). Due to the damper in the landing gear the stiffness of the landing gear becomes complex with the imaginary part $k_i = i\omega\gamma_D$ ($\gamma_D = 567$ N/m). It is easy to see from Eq. (5) that the deformation of the lander structure on a given material is deter-

mined by that part of the landing gear with the highest compliance or lowest stiffness.

6. Evaluation of the data measured on comet 67P

6.1. Signal types

There are a number of individual signals in the time series from comet 67P which look very similar to the touchdown signals in the LAMA tests (Faber et al., 2015). Two of them measured at Agilkia are shown in Figs. 7a and b. They are characterized by a time-length called contact time T_c in Hertzian contact mechanics, here $T_c = 7$ ms (Fig. 7a) and $T_c = 8$ ms (Fig. 7b). Other signals occur in the +Y-foot in x-direction at 0.735 s with $T_c = 22$ ms and at 0.98 s with $T_c = 8$ ms both at a contact resonance of 1.2 kHz. Further signals can be seen in the –Y-foot time series in x-direction at 0.65 s with $T_c = 10$ ms and $f_c = 1$ kHz, at 0.823 s with $T_c = 8$ ms and $f_c = 1$ kHz; in the +X-foot, x-direction at 0.429 s, $T_c = 7$ ms and $f_c = 1.1$ kHz and at 0.89 s with $T_c = 5$ ms and $f_c = 1.2$ kHz. Their common signatures are contact times $T_c \approx 10$ ms, negative wave-form close to a half-sinusoidal shape and amplitude-modulated with a frequency signal close to 1.1 kHz, see Tables 1–3. We interpret the modulation signals as contact-resonances of the sole in analogy to the signals measured in the LAMA tests. In the following sections, we discuss the half-wave signals as well as the contact-resonances.

Let us make some estimates before we analyze the data. From the time-of-flight data of the MUPUS hammering signal, the elastic surface modulus at the final landing site Abydos must be of the order of 10 MPa (Knapmeyer et al., 2015). Let us assume that there is the same surface modulus at Agilkia. The magnitude of the forces exerted by the foot soles on the comet soil were $P \approx 34$ N at Ag-

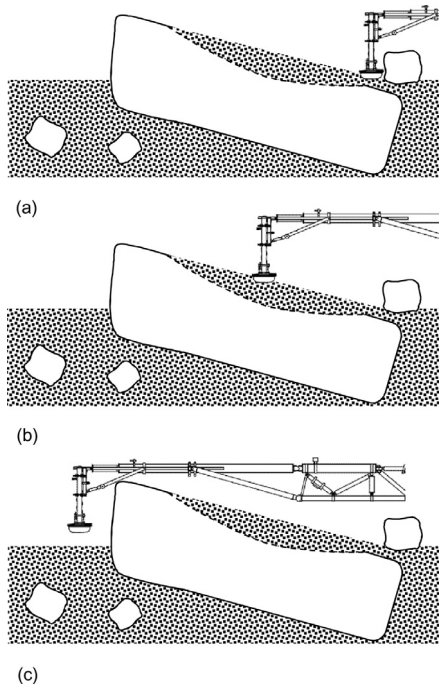


Fig. 6. Possible scenarios of the touchdown for the +Y-foot at the landing site Agilkia. The scenario (c) agrees with most of our finding; see text.

ilkia (Roll et al., 2016). Before plastic deformation of the comet surface sets in, there was an elastic deformation and this allows us to estimate the contact radius a_c ,

$$a_c = (3PR/4E^*)^{1/3}, \quad (6)$$

based on Hertzian contact mechanics (Johnson, 1985) to be $a_c \approx 8$ mm using $E^* = 10$ MPa as effective modulus between the sole and the comet surface material. The elastic deformation depth is $\delta = a_c^2/R \approx 0.3$ mm. Then we obtain a contact stiffness of $k^* = 2a_cE^* = 160$ kN/m, which is much larger than the stiffness of one arm of the landing gear ($k_{LG} = 13.3$ kN/m), but comparable to the stiffness of the sole $k_{sh} = 270$ kN/m. For a signal length of about $T_c = 0.1$ s (length of the strong signal of the +Y-foot), the angular frequency would be $\omega = 2\pi/T_c = 2\pi/0.1 \text{ s}^{-1} = 62.8 \text{ s}^{-1}$ and hence $\omega\gamma_D \approx 35.6$ kN/m. In addition, for the first contacts the damper of the landing gear was not activated (Roll and Witte, 2016), and therefore we neglect the contribution of the imaginary part to the compliance of the landing gear.

If the corresponding foot was fixed rigidly to the leg of the landing gear, the restoring force would be determined by its compliance and hence no information could be gained on the elastic modulus of the surface material, see Faber et al. (2015). However, if the ice screw mechanism in the foot is operating, the foot is decoupled during this time from the landing gear leg and the stiffness of the sole determines the reaction to the contact forces at Agilkia. The ice screws (Fig. 1b) were actuated at least partially upon the first landing of Philae. In the laboratory tests, this period lasted some 100 ms with a force of ≈ 20 N (Faber et al., 2015).

The signals of the +Y-foot are the strongest, exceeding those of the other two feet by a factor of ≈ 5 . Also only in the +Y-foot accelerometer, there are signals recorded at 1.3 kHz in the x-direction which are clearly above the noise level. As said in Section 5, the positional accuracy of the reconstruction of the landing site is ± 10 cm. Therefore it is quite feasible that a strut of leg 1 of the landing gear hit the boulder at its edge and not the sole (scenario (c) in Fig. 6). Then, the dangling foot caused the free oscillations of the sole at 670 Hz and the signals are amplified by the Q-factor of the resonance, which was measured on the spare foot sole to be $Q = 9$. Due to the nonlinear behavior of the stiffness of the spare sole versus loading force (see Appendix A3, Fig. A3.2), the generation of the second harmonic, i.e. the signal frequency at 1.3 kHz is quite natural. In a number of test experiments, it was checked whether such a scenario is possible and this seems to be the case, see Appendix A4, Fig. A4, and the video in the supplementary material. In several of these tests, it was easy to generate signal amplitudes comparable to and larger than the signal strength observed on comet 67P when the strut hit a styrofoam plate ($E_{r,cal} \approx 20$ MPa) at its edge.

6.2. Half-wave signals

Let us consider the half-wave sinusoidal signals as a periodic input disturbance of the oscillator shown schematically in Fig. 8, which depicts the mechanical equivalent model for the Coulomb friction force in the fixation ice screw mechanism, in addition to the inertia force by the mass of the foot. The dry friction element operates along the guidance system of rectangular tubes holding the foot soles. It acts as well on the ice screw fixture, which forces the screw rotation when the soles are pushed upward. Hence the dry friction attacks along a distributed mass and therefore the mechanical equivalent model in Fig. 8 is a simplification. There are a number of papers published in the 1960s and 1970s discussing oscillators with viscous and Coulomb friction elements whose results are now summarized in textbooks; see for example Nayfeh and Mook (1995). The paper by Levitan (1960) is particularly suited to describe the main features of the present problem. Treating the os-

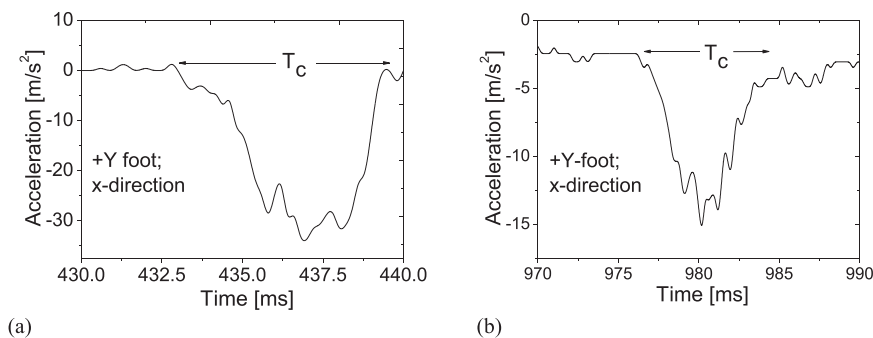


Fig. 7. (a) Signal at 437 ms of the +Y-foot, x-direction. The overall shape of the signal is sinusoidal with one negative half-wave of length $T_c = 7$ ms. Counting the number of oscillations in the signals, a contact-resonance at $\sim 1.1 \text{ kHz} \pm 0.1 \text{ kHz}$ becomes noticeable; (b) Signal at 980 ms of the +Y-foot, x-direction. The overall shape of the signal is sinusoidal with one negative half-wave of length $T_c = 8$ ms. Counting the number of oscillations in the signals, a contact-resonance becomes noticeable at $1.2 \pm 0.1 \text{ kHz}$.

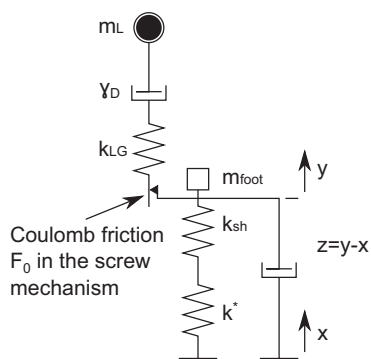


Fig. 8. Mechanical equivalent model for the Coulomb friction force in the fixation ice screw mechanism, in addition to the inertia force by the mass of a foot. The dash-pot element represents the viscous damping of the sole and the comet soil, here 7.1 Ns/m. Furthermore, m_L is the mass of the lander, γ_D is the damping constant of the landing gear (Roll et al., 2016), k_{LG} is the stiffness of the landing gear, k_{sh} is the stiffness of the sole, and k^* is the contact stiffness of the comet surface. The damping element parallel to k_{sh} and k^* is the damping of the sole determined by the Q-value of the contact-resonances; see text.

cillator of Fig. 8 as a point-mass system, the corresponding differential equation for the motion of the mass m_{foot} with the coordinate z relative ($z = y - x$) to the base plate with the coordinate x (representing the comet surface) is:

$$m_{foot}\ddot{z} + c\dot{z} + kz - F(t) = -m_{foot}\ddot{x} = m_{foot}\omega^2 \cos(\omega t + \phi) \quad (7)$$

for a sinusoidal excitation $x = x_0 \cos(\omega t + \phi)$. Here $F(t) = (4F_0/\pi) \sum_n (\sin(n\omega t)/n)$ is the Fourier series representation of the square wave frictional resistance curve $F_0 \times \text{sign}(\dot{z})$ and $F_0 = 2 - 20$ N is the magnitude of the frictional force (measured in spare foot assemblies in the course of the LAMA tests (Faber et al., 2015). Eq. (7) has been solved analytically for a steady state solution. The series $z(t) = \sum_n \{A_n \cos(n\omega t) + B_n \sin(n\omega t)\}$ (Levitan, 1960) was truncated at $n=5$ resulting in an error of less than 1% for the amplitude z . The following parameters determine the solution: (i) the friction damping factor $C_f = F_0/kx_0$ (with $1/k = 1/k^* + 1/k_s$), (ii) viscous damping ratio $\alpha = c/c_0$ (with $c_0 = 2m_{foot}\omega_0$), (iii) ratio β of the excitation frequency/eigenfrequency, here $(\pi/T_c/\omega_0)$, and (iv) $x_0 =$ forced excitation amplitude of the base plate $x_0 \times \cos(\omega t)$. The parameters are $\alpha = 9.26 \times 10^{-2} \approx 0.1$; $\beta = 7.48 \times 10^{-2}$. The ratio C_f is difficult to estimate. Because the accelerometer in each sole is firmly attached to the soles, we can equate the soles' amplitudes $x_0 = b/\omega^2$ with the excitation amplitude x_0 . Here, a typical value is $b \approx 20 \text{ m/s}^2$, see Tables 1–3, and $\omega/2\pi$ is the contact-resonance frequency $\approx 1.1\text{--}1.2$ kHz. This yields $x_0 \approx 0.4 \mu\text{m}$. The stiffness of the springs k^* and k_s in series is then $k \approx 150 \text{ kN/m}$ (see Section 6.3.2). Finally with $F_0 \approx 20$ N, one obtains $C_f \approx 330$ as an upper value and with $F_0 \approx 2$ N $C_f \approx 33$ as a lower value. Reading the parameterized data shown in Fig. 4 of Levitan (1960), we conclude that the peak transmissibility, i.e. the ratio of y_0/x_0 is close to 1. The oscillating forces acting on the sole are not influenced by the ice screw mechanism because they are smaller than the friction forces, and hence the soles can be regarded as an isolated system as long as the screws are not stopped. This finding allows us to apply the theory of Faber et al. (2015), to invert the data where the compliance of the foot sole compensates the restoring force when contacting the comet instead of the leg of the landing gear. In that case $F(x)$ is the restoring force in the contact sole-comet surface, i.e. $F(x) = (4/3)R^{1/2}E_r^*x^{3/2}$ for an elastic Hertzian contact. For a plastic contact, this force is given in a first approximation by $F(x) = A \times \sigma_c$ where A is the contact area and σ_c is the compression strength. In view of the permanent indentations Philae left behind at Agilkia, it is appropriate to assume that the elastic-plastic yield limit was exceeded by each

foot and that the further deformation occurred then only by plastic deformation, i.e. that the surface of the comet material was loaded so that the individual signals are caused by the crushing of the porous structure similar to the results of the KOSI experiments (Grün et al., 1993; Kochan et al., 1998; Kochan et al., 1989; Thomas et al., 1994). Here, the simplified assumption is made that the compression strength is a constant. Applying Eq. (3) in Faber et al. (2015) yields:

$$\begin{aligned} |b_{\max}| &= K_0 \sqrt{\left(\frac{1}{m_{foot}} - \frac{\omega^2}{k_{sh}}\right)^2 + \frac{\omega^2}{\gamma_{sh}^2}} = K_0 \sqrt{\frac{1}{m_{foot}^2} \left(1 - \frac{\omega^2}{\omega_0^2}\right)^2 + \frac{\omega^2}{\gamma_{sh}^2}} \\ &= \frac{K_0}{m_{foot}} \sqrt{\left(1 - \frac{\omega^2}{\omega_0^2}\right)^2 + \frac{\omega^2 Q^2}{\omega_0^2}}. \end{aligned} \quad (8)$$

In laboratory tests the Q-value of a spare sole's free oscillations was measured to be $Q=9$, and it remained unchanged when the sole was firmly immersed in Aerosil (appendix, Table A5) as an analog material for the loose comet soil. In Eq. (8), the angular frequency ω is $\omega = \pi/T_c$ where T_c is the contact time, $\omega_0 = 2\pi \times 670 \text{ s}^{-1} = 4.2 \times 10^3 \text{ s}^{-1}$ is the free resonance frequency of the sole, and $m_{foot} = 0.82 \text{ kg}$ is the mass of a foot. Furthermore, the damping constant of the sole is $\gamma_{sh} = k_{sh}/Q\omega_0 = 7.1 \text{ Ns/m}$. As said above, the contact times are of the order of $T_c \approx 10 \text{ ms}$ yielding $\omega = \pi/T_c = 3.1 \times 10^2 \text{ s}^{-1}$. Inserting these parameters and because $\omega \ll \omega_0$, Eq. (8) leads to:

$$K_0 \approx \frac{|b_{\max}| \times m_{foot}}{1.2} = A \times \sigma_c. \quad (9)$$

The acceleration values b_{\max} are between -10 and -34 m/s^2 . This yields magnitudes of impact forces K_0 between 7 and 23 N. This force corresponds to the measurement of the forces obtained in a spare foot, see above, and also to the estimate of the force exerted by the effective mass of a landing gear leg at touchdown (Roll et al., 2016).

For predominantly plastic deformation, the maximal contact radius is given by the radius of the sole provided that the whole sole surface contacts the comet surface. This yields a maximal contact area of $A \approx 0.016 \text{ m}^2$ if the two soles of a foot touch down at the same time. Hence the compression strength $\sigma_c = K_0/A$ is between 0.43 and 1.5 kPa and will be correspondingly larger if the contact area is smaller given by the particles of the regolith at Agilkia with diameters down to cm size (Mottola et al., 2015). This yields a contact area of $A = 2 \times 10^{-3} \text{ m}^2$ and hence compression (or crushing) strengths between 3.5 kPa and 12 kPa. These values are indeed comparable to the estimates of $\sigma_c = 2 \text{ kPa}$ given in Roll et al. (2016), where the magnitudes of the forces were estimated that the lander soles exerted onto the comet surface based on a detailed mechanical model of Philae. Here, we derived the forces from the acceleration data at the Philae feet measured in situ.

In such a scenario the CASSE signals are caused by the forces exerted on the sole when crushing and pushing the assembly of the individual particles of the comet regolith further into the comet surface. One should keep in mind that Eqs. (7) and (8) are based on a simplified model and it is re-assuring that all three approaches to determine the compression or crushing strength at the Agilkia site yield the same result within a factor of three.

6.3. Philae's sole resonances

Before we analyze the contact-resonance data from comet 67P, we discuss the free and the contact-resonances of the sole of a spare foot which were determined by calibration experiments and are described in detail in Appendix A5.

6.3.1. Free resonances

The free resonance of a spare foot sole was measured at room temperature by tapping on the lid of the sole, recording the output of the accelerometer either with a digital oscilloscope or by the B&K “Pulse” device with corresponding software which powered the sensor and which recorded the signals as well, see Appendix A5. The free resonance averaged over 10 measurements was 540 ± 14 Hz, a value obtained repeatedly in many additional individual measurements.

From Eq. (A5) (Appendix A5), it can be seen that the resonance frequency is proportional to the square root of the Young modulus of the sole, i.e. $\omega \propto E_{sh}^{0.5}$. The Young modulus of the polymer component of the composites may increase considerably with decreasing temperature, depending on whether the temperature range is close to the glass transition temperature of the polymer. According to the housekeeping data of the CASSE sensors, the temperatures of the feet were roughly -100 °C. Literature data show (Amash and Zugenmaier, 1997; Bansemir and Haider, 1998; Shokrieh et al., 2012) that the elastic modulus of GFC materials increases by a factor of ≈ 1.7 for a temperature of $T \approx 200$ K compared to the value at room temperature. Therefore, one can expect that the free resonance-frequency increases by a factor of $\sqrt{1.7} \approx 1.3$ relative to room temperature, i.e. from $f_r = 540$ Hz to about 700 Hz.

6.3.2. Contact-resonances

From the Fourier spectra of the accelerometer signals, one can clearly see frequency bands below and above 680 Hz; see Figs. 2b–4b and Table 1. As said above, we interpret these frequencies as contact-resonances of the foot soles with variations in the boundary conditions due to the variations in the contact mechanics when the soles encountered the surface of 67P at Agilkia. The oscillations of the soles were excited by the time-varying forces of multi-asperity contacts with the pebbles of the comet surface and/or with the surface of the boulder hit, or by the strut hitting the edge of the boulder.

Eq. (4) describes in a quite general way the contact-resonances ω_{th} as a function of the contacted masses involved and of the contact stiffness k^* . Mass loading of the soles leads to a decrease of the contact-resonances whereas stiffening by restoring forces leads to their increase (Vidic et al., 1998). Calibration curves were obtained by measuring the contact-resonance of a spare foot-sole resting on materials of known reduced elastic moduli. The contact-resonances were excited by tapping on top of the lid with the sole having contact to the material tested or by fall tests; see Appendix A5.

Material constants, i.e. Young’s modulus E , shear modulus G , and the Poisson ratio ν of the calibration materials were measured by ultrasonic velocity measurements and by density measurements. From these data the reduced Young’s modulus $E_{r,cal} = E/(1 - \nu)^2$ of the material was determined; see Table A5 in the appendix. The normalized contact-resonance frequency f_c/f_r is plotted as a function of the reduced modulus of the calibration materials, $E_{r,cal}$; see Fig. 9.

From Tables 1 to 3, we read that most of the contact-resonances measured on comet 67P extend from ≈ 1.1 to 1.2 kHz. That corresponds to $f_c/f_r = 1.2/0.68 \approx 1.8$, and from Fig. 9 one infers a corresponding reduced modulus $E_{r,cal} \approx 2$ GPa. In order to calculate the corresponding contact stiffness, one needs the contact radius as well, as seen in Eq. (3). In our case $R = 0.2$ m is the curvature radius of the foot sole, $P = 4.92$ N is the load, i.e. the static force exerted by the weight of one leg of the landing gear on the calibration sample via the sole (housing the accelerometer), which was measured by aid of a balance. In Eq. (3), E_r^* is the effective modulus of both contacting structures, the foot sole with its measured stiffness and the calibration materials that are assumed to be homogeneous. This should hold for the materials with a smooth sur-

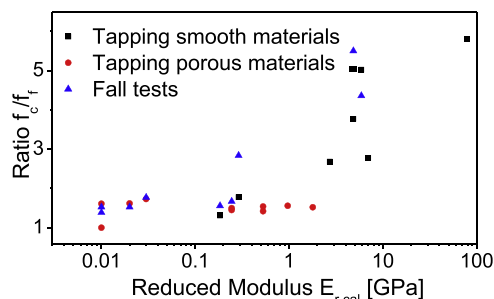


Fig. 9. Normalized contact-resonance frequency f_c/f_r versus reduced elastic modulus $E_{r,cal}$ of the calibration materials. Squares represent contact-resonance values obtained by tapping, circles are data for porous materials, and triangles represent data from fall tests. The data are listed in Table A5 in Appendix A5. The steep increase in contact stiffness occurs when the contact stiffness is comparable to the sole stiffness (color online).

face. Let us find an equivalent volumetric material with a reduced modulus E_{equi} that develops the same contact radius as the shell structure of the foot sole when pressed into the calibration material. Obviously $E_{equi} = k_{sh}/2a_c$ must hold (Eq. (3)). Using Eq. (2), i.e. $1/E_{r,eff}^* = 2a_c/k_{sh} + 1/E_{r,cal}$ and inserting $1/E_{r,eff}^*$ into Eq. (6), one obtains an algebraic equation for the contact radius. The solution of this equation yields $a_c \approx 3$ mm and the corresponding contact stiffness at $f_c/f_r = 1.8$ is $k^* = 2a_c E_{r,eff}^* \approx 157$ kN/m ($E_{r,eff}^* = 26.3$ MPa). That means that the maximal change in the dispersion curve of Fig. 9 occurs when $k_{sh} \sim k^*$, which is physically plausible.

Let us apply this finding to the situation on the comet. We obtain the same result if the contact radius remained the same. However, this cannot be expected. For the contact radius one has to take rather the sole radius, i.e. a factor $50/3 \approx 16.7$ larger whereas the sole stiffness should increase to ≈ 270 kN/m (see Appendix A3). This translates into a surface modulus of about 3 MPa.

In case of multi-asperity contacts, like on an ensemble of pebbles on the comet, or in case of very porous and rough surfaces, like volcanic rock, the contact radius can no longer be calculated with Eq. (6), and as a result the inversion of the data as done above is no longer possible. This situation is even more pronounced for the fall tests on such materials (data marked with triangles in Fig. 9).

7. Discussion

In porous materials, both the elastic moduli as well as the fracture mechanical parameters such as tensile strength, compressive strength, and fracture toughness are reduced. During the preparation phase of the Rosetta mission an effort was undertaken to estimate the compressive strength of comets by using the ratio of the strength/elastic modulus structure for a foam-like structure with open cells (Gibson and Ashby, 1997; Möhlmann, 1996):

$$\sigma_c/E_c = 0.03(\rho_p/\rho_s)^2(1 + \sqrt{\rho_p/\rho_s})^2. \quad (10)$$

Here, σ_c is the elastic stress for compression failure and ρ_p and ρ_s are the mass densities of the comet nucleus materials with porosity and for the pore free material, respectively. E_c is the Young’s modulus of the comet material. Inserting for the porosity $(1 - \rho_p/\rho_s) = 0.7 - 0.8$, one obtains $2.5 \times 10^{-3} < \sigma_c/E_c < 6.5 \times 10^{-3}$ and for $\sigma_c = 8$ kPa, this yields 1.2 MPa $< E_c < 3.2$ MPa. This range shows the large influence of the porosity.

Similar expressions to Eq. (10) have been derived for cellular materials (Ashby, 1983; Gibson and Ashby, 1997). Based on the proposal that the glue between the particulates of the comet regolith might be ice (Greenberg et al., 1995; Möhlmann, 1996) and considering the high porosity, the comet surface material may be viewed as a cellular material with the ice as the walls between

the regolith particles. Let us briefly discuss the consequences of such an approach. There are experimentally determined master curves for cellular materials for the ratio of the elastic collapse strength/elastic modulus of the cells by cell-wall buckling, i.e. crushing (Ashby, 1983). Again for a porosity of 0.7–0.8, this ratio is $1.7 \times 10^{-3} < \sigma_c/E_c < 7.9 \times 10^{-3}$ i.e. for $E_s = 8$ GPa (ice) (Fellin, 2013), we obtain $13 \text{ MPa} < \sigma_c < 63 \text{ MPa}$. For stresses beyond 4 MPa, the deformation of the material becomes non-linear, but it is still elastic, i.e. the strain is recovered when unloaded.

If the cell walls can be deformed plastically, which ice can undergo, there is a yield strength σ_{pl} that depends on porosity. Again there are master curves (Ashby, 1983), and for a porosity of 0.7–0.8, the relative plastic yield strength σ_{pl}/σ_w is $2.4 \times 10^{-2} < \sigma_{pl}/\sigma_w < 5.7 \times 10^{-2}$. It is not straightforward to select the correct parameter for the strength σ_w of the ice walls, because they will undergo both shearing and compression when loaded. From the tables in Fellin (2013), we find the lower limit $\sigma_w \approx 1 \text{ MPa}$ and $\sigma_w \approx 10 \text{ MPa}$ as an upper limit. This entails $\sigma_{pl} \approx 24 \text{ kPa}$ as a lower limit and $\sigma_{pl} \approx 57 \text{ kPa}$ as an upper limit for $\sigma_w = 1 \text{ MPa}$ and $\sigma_w = 10 \text{ MPa}$, respectively.

Independent of the question whether ice serves as glue between the regolith particles, brittle cellular porous materials may fail in compression by crushing. After elastic deformation followed by crushing, there is a plateau regime of stress versus strain during which energy is absorbed upon further straining the material and eventually densification sets in at larger strains ε (see Fig. A6). Such a scenario has taken place according to the analysis of the energy balance of the landing events (Biele et al., 2015; Roll et al., 2016). As an example for porous ceramic Al_2O_3 with a porosity of 80%, the ratio is $2 \times 10^{-3} < \sigma_c/\sigma_w < 10^{-2}$ (Dam et al., 1990), which entails a crushing strength of $20 \text{ kPa} < \sigma_c < 100 \text{ kPa}$ for $\sigma_w \approx 10 \text{ MPa}$, and $2 \text{ kPa} < \sigma_c < 10 \text{ kPa}$ for $\sigma_w \approx 1 \text{ MPa}$.

The fracture of a material is sensitive to defects such as pre-existing cracks, inclusions or large cells or voids in cellular materials. This holds in particular for the tensile strength of materials. Defects act as stress concentrators. This is taken into account by the concepts of fracture mechanics (Lawn, 1993) which are also applied in rock mechanics, see for example Hatzor and Palchick, 1997. Again there are master curves for the fracture stress σ for porous materials (Ashby, 1983), which for a porosity of 80% give

$$\sigma \approx 10^{-2} \sigma_w \sqrt{d/L_c}. \quad (11)$$

Here, σ is the fracture stress, L_c is the length of the cells and d is the linear defect size. Eq. (11) holds for $d > L_c$. The smallest cell size for the comet regolith is $L_c = 0.4 \text{ mm}$ (Mottola et al., 2015). Let us assume we have $d = 10 \text{ cm}$. This yields a fracture stress of 6.5 kPa if we assume again that the cell walls are ice, i.e. $\sigma_w \approx 10 \text{ MPa}$. It should be mentioned that Greenberg et al., 1995, stated that a fracture mechanics approach would be the correct way of describing the fracture strength of comet materials.

Similar considerations and relations exist for the elastic moduli and fracture strength of ceramics before sintering which are either slurries or dry-pressed powders, so-called green bodies (Kendall et al., 1987; Kendall et al., 1986). Green ceramic bodies have an appreciable amount of porosity and also, like assumed for the comet material, the individual particles in the unfired material contact each other at certain points, where interatomic forces hold the ensemble of particles together (Tabor, 1977). They deform the particles at the contact points elastically. The energy needed to separate two particles is $a_{cp}^2 \times \Gamma$ where a_{cp} is the radius of the contact points and Γ is the surface energy. When the two particles are separated, the elastic energy is released which reduces the total energy needed for separation. The number of contacts in the ensemble with surface area πa_{cp}^2 depends on the overall porosity. Experimentally this dependence was determined to be proportional

to $(\rho_p/\rho_s)^z$ with z being 2, 3, and 4 (Carneim and Green, 2001) instead of the almost squared power dependence of Eq. (10) and the master curves cited above. This makes the relations very sensitive to the actual porosity at small values of ρ_p/ρ_s (Arnold and Möhlmann, 2009).

In summary, it is the porosity which determines the elasticity and strength for small ρ_p/ρ_s (Ashby, 2006; Leite and Ferland, 2001). The material of the cell walls and the binding by surface forces, i.e. the surface energy, play a minor role.

8. Comparison to other relevant data

Large cracks and features of irregular polygonal structure with a size of the order of some m to some 100 m have been observed on comet 67P (El-Maarry et al., 2015). Smaller cracks of sizes comparable to and smaller than the diameter of Philae's soles exist as well. In fact fractures and cracks are ubiquitous at grain and boulder scales (Bibring et al., 2015).

Tensile or failure strengths for comet 67P of $\approx 100 \text{ Pa}$ have been reported for dust overhangs (Thomas et al., 2015) much smaller than the estimate for the tensile strength estimated in the previous section (6.5 kPa), which might be due to the still higher porosity in the dust overhang. Groussin et al. (2015) discussed in detail the various strength values derived from the airfall of the overhangs, shear strengths from adhesion and rolling of boulders (4 Pa), and eventually the compression strength derived from the depression depth the lander soles left behind at Agilkia ($\approx 16 \text{ kPa}$). One also finds in this paper a table summarizing tensile strengths, shear strengths and compressive strengths for cometary materials and the corresponding references.

A tensile strength of 10 Pa already influenced the further motion of Philae at Agilkia in modeling the landing event (Roll and Witte, 2016). Estimating the forces acting on the soles upon landing, Roll et al. (2016) derived a compressive strength at Agilkia of 2 kPa. Finally, a hardness value of 4 MPa has been reported for the MUPUS experiment carried out at Abydos (Spohn et al., 2015).

Thus, the experimental data reported so far for comet 67P indicate that the tensile strengths are of the order $\approx 100 \text{ Pa}$, whereas compressive strengths are much larger, i.e. of the order of up to 10 kPa and at Abydos up to some MPa, see also Basilevsky et al. (2016).

Let us compare these data with the KOSI laboratory experiments (Kochan et al., 1998; Thomas et al., 1994). The crushing strength of a porous ice–mineral composite with an olivine content of 3.4% was examined. Most interesting was the observation that the crushing strength increased with sintering time reaching a value of $\approx 0.5 \text{ MPa}$ after ≈ 3 days at 253 K. With increasing mineral content the crushing strength increased slightly. The neck growth between the particles and hence the stability of the sintered material was estimated as well. In about 10^6 years the neck radius would be about equal to the particle radius, and the strength of the composite would then be fully developed. Different specimens were produced with grain sizes around 1 mm, and they contained H_2O and CO_2 ice with 15% weight percentage. The minerals added were olivine and montmorillonite. The overall porosity was 49–63%. The measured hardness was 0.15–1 MPa. As said earlier, in these measurements gradual crushing of the KOSI material was observed which manifested itself by oscillating strength values with increasing penetration by the indenter. That fracture mechanical concepts should be applied to describe the strength of comet analogue materials and eventually comet material, was clearly spelled out in a number of papers given at the Int. Workshop on Physics and Mechanics of Cometary Materials which took place in Münster, Germany in 1989 (Proceedings Vol. SP-302, ESA, Paris, France).

A lot of data have been published concerning the properties of ice and snow, see for example data in Fellin (2013).

Petrovic gave a detailed account of the mechanical properties of ice (Petrovic, 2003). The tensile strength of ice varies from 0.7 to 3.1 MPa and the compressive strength varies from 5 to 25 MPa over the temperature range -10 °C to -20 °C. The ice compressive strength increases with decreasing temperature and increasing strain rate, but ice tensile-strength is relatively insensitive to these variables.

There exist quite a lot of laboratory experiments and theoretical estimates to gain insight into the strength of dust aggregates related to comets. One finds values for tensile strengths of the order of some 10 Pa with exceptions of up to some 10 kPa. However, we refrain from summarizing these papers in detail and refer to Luding (2008), Meisner et al. (2012), Musiolik et al. (2017), Skorov and Blum (2012), and references therein.

9. Summary and conclusion

The analysis of the CASSE acceleration data yields compression strengths of ≈ 10 kPa for the comet surface material. This is in line with the data previously published considering the forces exerted by the lander on the comet surface at Agilkia (Roll et al., 2016). In our analysis, these forces were derived from the signals of the accelerometers mounted in the foot soles of Philae's landing gear. Assuming that the same relations known for highly porous natural and engineering materials apply to the surface material of comet 67P, its elastic modulus should be of the order of a few MPa at Agilkia. Such a value was indeed found by the evaluation of time-of-flight data during the MUPUS hammering at Philae's final landing site Abydos (Knapmeyer et al., 2015).

It is the porosity which determines the elasticity and the strength of a porous material with large porosity. On the one hand, the porosity reduces the number of contacts or the coordination number between the individual constituents of the comet agglomerate material, and on the other hand large pores act as stress concentrator initiating failure upon loading. This concept is also applied in rock mechanics (Hatzor and Palchick, 1997). The large variations of strength values reported on comet 67P from a few tens of Pa (Groussin et al., 2015; Thomas et al., 2015) to several MPa (Spohn et al., 2015) can be explained by local variations in porosity.

Acknowledgments

With shock and grief the co-authors learnt that Prof. Dr. D. Möhlmann passed away on September 28th 2016, 2 days before the end of the Rosetta mission. In his active time at the DLR-Institute of Space Simulation in Cologne, Germany, he was responsible as the first one of the three SESAME PIs for the planning and integration of the three instruments CASSE, DIM and PP into the Philae experiment SESAME. The co-authors express their deep gratitude for his outstanding contributions to our common project.

We thank R. Birringer and A. Steinbach, Department of Physics, Saarland University for the measurement of the stiffness of a flight-spare foot-sole. We also thank G. Falk and W. Possart, both Department of Materials, Saarland University, for providing the tuffstone (with the porosity value) and the polyurethane calibration samples, respectively. Likewise, we are grateful for the porous rock samples with porosity values provided by M. Prasad, School of Mines, Golden, CO, USA. W. A. thanks K. Samwer, I. Phys. Institut, Georg-August Universität Göttingen, and J. Turner, Department of Mechanical Engineering, University of Nebraska, Lincoln, NE, for many helpful discussions on various aspects of contact-resonances, and also G. H. Schwehm, ESA-ESTEC, Noordwijk, Netherlands for helpful discussions on the results of the KOSI experiments. We thank N.A. Burnham, Worcester Polytechnic Institute, MA for a critical reading of the manuscript. Last but not least, we thank W.

Gebhardt and R. Licht for their invaluable contributions in developing the CASSE instrument at Fraunhofer IZFP.

Rosetta is an ESA mission with contributions from its member states and NASA. Rosetta's Philae lander is provided by a consortium led by DLR, MPS, CNES and ASI. SESAME is an experiment on the Rosetta lander Philae. It consists of three instruments CASSE, DIM and PP, which were provided by a consortium comprising DLR, MPS, FMI, MTA EK, Fraunhofer IZFP, Univ. Cologne, LATMOS and ESTEC. All data will be made available via the ESA Planetary Science Archive.

Appendix

A.1. Elastic modulus of the glass-fiber composite sole

The elastic parameters of the GFC sole were obtained from ultrasonic velocity measurements at frequencies 2–3 MHz using broadband excitation. They yielded a longitudinal velocity of $v_L = 3330$ m/s. With a density of $\rho = 2.3 \times 10^3$ kg/m³, this gives $L = 25.55$ GPa, where $L = v_L^2 \times \rho$ is the so-called longitudinal modulus. Likewise, the measurement of the shear velocity gave $v_S = 1910$ m/s. This yields a shear modulus $G = v_S^2 \times \rho = 8.4$ GPa and with $\nu = [(L - 2G)/2(L - G)]$ a Poisson ratio of $\nu = 0.255$. Therefore, the E-modulus is $\nu = 2(1 + \nu)G = 21.1$ GPa and the reduced modulus is $E^* = E_{sh}^* = 22.6$ GPa. These values are close to literature values of $E = 20$ GPa (Schwartz, 1992). Due to high attenuation caused by scattering of ultrasound at the composite structure, it was not possible to determine the anisotropy factor of the GFC material in the plane of the woven fabric.

A.2. Height of the boulder

The length of the shadow of the boulder hit is on its left side (West) about $w \approx 0.4$ m; see Fig. 5. The sun stood at an elevation of $\vartheta = 40^\circ$ to the plane of the landing site (Mottola et al., 2015). This yields a maximal height of the boulder

$$H = w \times \tan \vartheta \approx 0.34 \text{ m} \quad (\text{A1})$$

Since the edge of the boulder is rounded and flattened from West to East (left to right in Fig. 5) and eventually dives into the ground, there is no single height. At the part where the landing gear probably hit the boulder, the height is only 15–20 cm.

A.3. Sole stiffness

Analytical estimate of the sole stiffness

The stiffness of the sole including the foot structure was estimated to be 173 kN/m in the appendix (i) in Faber et al. (2015), based on the collection of equations in Young and Budynas (2002). An analytical expression for the stiffness of a spherical shell is given by Mansoor-Baghaei and Sadegh (2011):

$$k_{sh} = 2.3 E_{sh} t_{sh}^2 / R_{sh} \sqrt{1 - \nu_{sh}^2}. \quad (\text{A2})$$

Here, E_{sh} is the elastic modulus of the shell, t_{sh} is its thickness, and R_{sh} is the curvature radius of the shell. Inserting for the glass-fiber $E_{sh} = 21.1$ GPa with a Poisson ratio of $\nu_{sh} = 0.26$, $t_{sh} = 1$ mm, and $R_{sh} = 0.2$ m, yields $k_{sh} = 251$ kN/m. In an additional work (Mansoor-Baghaei and Sadegh, 2015), the stiffness of an ellipsoidal shell was given as

$$k_{sh} = 8(D_b E_{sh} t_{sh} K)^{1/2}. \quad (\text{A3})$$

Here, K is the Gaussian curvature in loading location and D_b is the bending stiffness of the shell defined as

$$D_b = E_{sh} t_{sh}^3 / 12 \sqrt{1 - \nu_{sh}^2}. \quad (\text{A4})$$

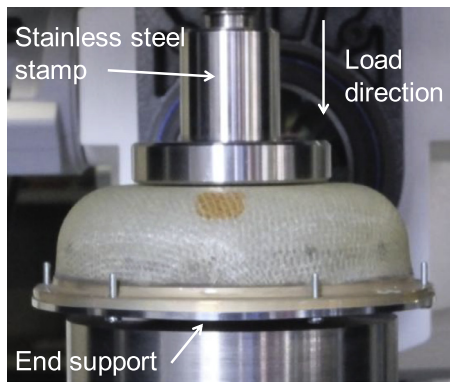


Fig. A3.1. Photograph of the sole mounted in the Instron tensile-compression device (color online).

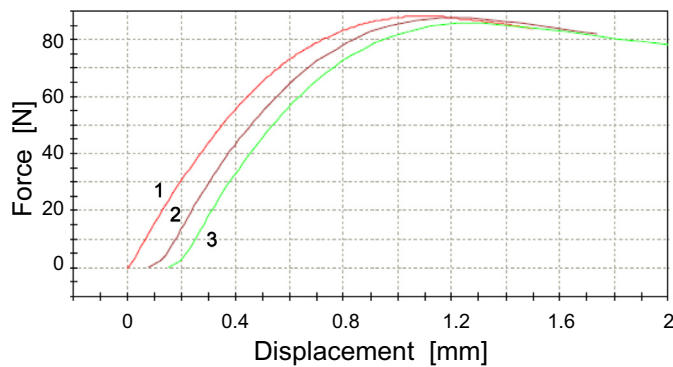


Fig. A3.2. Load force versus displacement for a Philae landing sole. The sole was loaded at two velocities: 1 mm/s (red curve 1) and 0.1 mm/s (brown 2, and green curve 3) (color online).

The Gaussian curvature is given by $K=1/R_1R_2$. Here, $R_1=200$ mm and $R_2=50$ mm (see Fig. A2 for the foot measures in Faber et al. (2015)). Inserting these numbers into Eqs. (A3) and (A4) yields $D_b=1.82$ Nm and $k_{sh}=495$ kN/m, almost the double value of Eq. (A2).

Measurement of the sole stiffness

In view of the difference in the above estimates for k_{sh} , the stiffness of a spare sole foot with a mounted B&K accelerometer was measured. The lid of the sole was screwed on. In an Instron 5546 tensile test machine the sole was loaded by compression using a stamp of 50 mm \varnothing made of stainless steel; see Fig. A3.1. With a 50 μ m thin feeler and by sideward palpation at the highest load of ≈ 90 N, the contact radius was determined to be $a_c=7.5$ mm (± 1 mm). For the loading procedure, the following termination criteria were pre-defined: Force up to 150 N and displacement up to 1.5 mm, respectively 2 mm (green curve), whatever value was reached first. From the initial slope of the compressive force versus displacement, a stiffness of $k_s \approx 160$ kN/m was determined for all three tests (Fig. A3.2) very close to the earlier estimate of 173 kN/m (Faber et al., 2015). At the highest load the sole was dented. However, when unloaded, the dent-in was elastically fully restored.

From Eqs. (A2), (A3) and (A4), one reads that the sole stiffness is proportional to its elastic modulus. In the main text the change of the modulus for temperatures down to 200 K is estimated. It is increased by a factor of 1.7 compared to room temperature. Therefore, the stiffness should increase to $k_{sh} \approx 270$ kN/m.

A.4. Fall tests on the edge of a hard-polystyrene foam plate of 20 mm width

A number of fall tests were carried out where the arm of the landing gear fell on the edge of styrofoam plate. Polystyrene hard foam has an elastic modulus of about 20 MPa; see Table A5. These tests served to simulate the scenario depicted in Fig. 6c. The fall height was 4.1 cm. For this test, the ice screw was blocked from operating. The contact resonances excited at 2 kHz fit well on the dispersion curve of Fig. 9 with $f_c/f_f=3.7$ and $E_{r,cal}=5.9$ GPa. The absolute values of the acceleration were even larger than on comet 67P for the landing leg +Y. The contact time for the 2 kHz oscillations is $T_c \approx 3\text{--}4$ ms. Applying the same procedure as in Section 6.3.2 to calculate an equivalent elastic modulus for the sole for $P \approx 0.5 \text{ kg} \times 600 \text{ m/s}^2 = 300 \text{ N}$, $k_{sh}=160$ kN/m, and $E_{r,cal}=5.9$ GPa yields $a_c \approx 7.5$ mm and $E_f^*=10.7$ MPa. With these values and $m=1.67$ kg for the leg, we estimated the theoretical T_c using Eq. (11.24) in Johnson (1985), despite the fact that this equation is an oversimplification for our case. One obtains $T_c=7.5$ ms in reasonable agreement with the observation. Before and after this slight touch, the signal frequency was 540 Hz, i.e. that of free resonances of the sole.

A.5. Sole resonances

Analytical estimate of the free sole resonance

At least the measured free resonance should be compared to a theoretical calculation. Assuming that the soles are half-domes, the frequency of the lowest eigenmode has been calculated by Reissner (1946):

$$\omega = 2.98 \frac{t_{sh}}{a_s^2} \left(\frac{E_{sh}}{\rho(1-\nu^2)} \right)^{0.5} \times \left(1 + (1+\nu)(0.9 - 0.2(1+\nu)) \frac{h^2}{t_{sh}^2} \right)^{0.5}. \quad (\text{A5})$$

Here, E_{sh} is the elastic modulus of the sole, ρ is its density, ν is the Poisson ratio of the sole material, and t_{sh} is its thickness. The parameter a_s is the radius of the spherical segment of the dome and h is its height. A fit of the real oblate form of the foot sole to the half-dome yields the parameters $a_s=17.5$ mm and $h=1.9$ mm. The parameters $E_{sh}=21.1$ GPa, $\nu=0.26$, $\rho=2.3 \times 10^3$ kg/m³, and $t_{sh}=1$ mm gives for the lowest mode $\omega=6.064 \times 10^4 \text{ s}^{-1}$, and $f=9.7$ kHz. The accuracy for the input parameters is not very high and therefore $f=9.7$ kHz is only an approximate value. In addition, the sole is mass-loaded by the mass of 28 g of the B&K accelerometer, which reduced the resonance frequency. This effect was measured in the development stage of the sole transmitters and receivers. A sole with a measured resonance at 1.85 kHz without mass, reduced its resonance frequency to 510 Hz when mass loaded (Arnold et al., 2004). Finally, finite element modeling gave results very close to the measured values (Krause, 2007).

Calibration measurement of the sole contact-resonances

A number of calibration experiments were carried out in order to determine the free and the contact-resonance frequency of a flight spare foot with a sole that was built identically to the flight model. For all measurements, the B&K 4506 (Deltatron) accelerometer was powered according to the specification of the manufacturer, i.e. 2–10 mA at 18–30 V for each of the three axes. The sensitivity according to the data sheet of B&K is 10 mV/(m/s²). Before and after each round of measurements, the sensitivity was checked using the calibration vibrator-exciter 4294 of B&K. This exciter provided amplitudes of 10 m/s². Each measurement was repeated about 10 times and the data were averaged and standard deviations were determined.

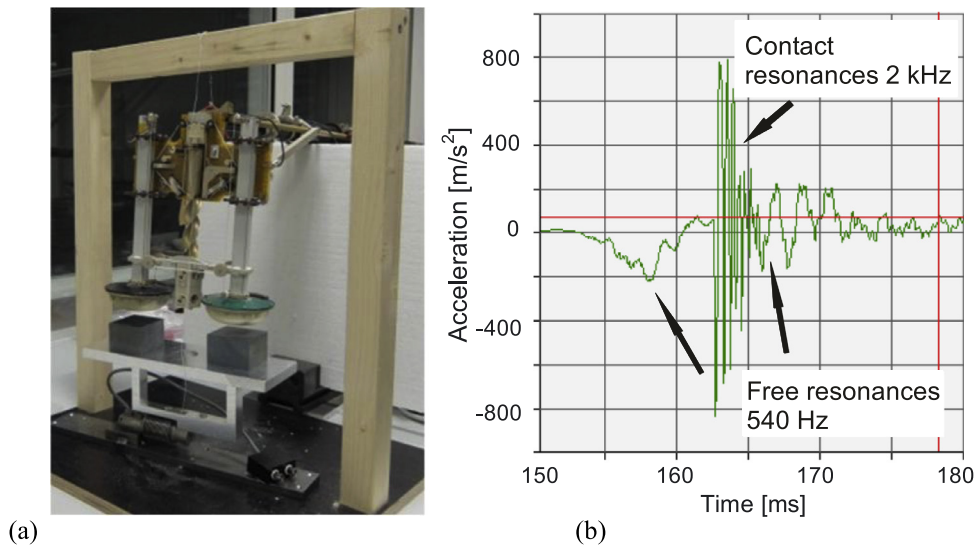


Fig. A4. (a) Fall test where the strut of the landing gear falls on the edge of an upward positioned hard-styrofoam plate with $E_{r,cal} = 20 \text{ MPa}$; (b) The sole of the foot touches for about $T_c \approx 3\text{--}4 \text{ ms}$ a cube made of polyamide ($E_{r,cal} = 5.9 \text{ GPa}$) which leads to excitation of contact resonances $f_c = 2 \text{ KHz}$ (color online). A video of the fall test was taken at a rate of 150 frames/s; see supplementary material). Its length of 38 s corresponds to 7.6 s.

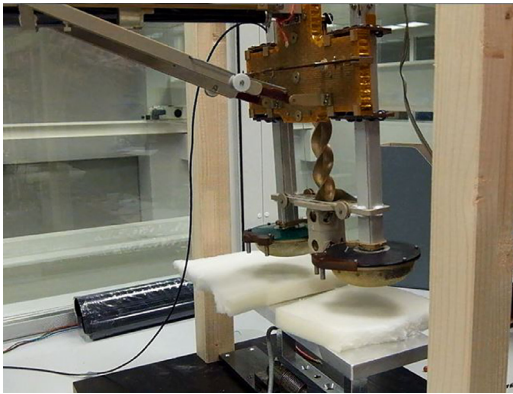


Fig. A5. Fall test on hard styrofoam samples. The arrangement was such that the ice screw mechanism could operate freely. Fall heights to measure the dispersion curves were 3–5 cm. High speed videos were taken in order to measure the velocity. In the aluminum table on which the styrofoam samples rest, a load cell was integrated in order to measure the impact forces (color online).

Excitation of the sole resonances by tapping

In a first round of measurements, the soles were excited to oscillations by tapping them with a pencil on their lid when they rested on the calibration sample. Elastic moduli, i.e. Young's modulus E , shear modulus G , and the Poisson ratio ν for the calibration materials were evaluated from ultrasonic time-of-flight data and the density. In case of Aerosil and the foam material, a compression test was carried out with a spare sole yielding directly the reduced modulus $E_{r,cal}$. The free resonance f_f was measured by tapping the sole without contacting the sample, respectively by a small loudspeaker which was placed below the sole's center. The result was $f_f = 540 \pm 14 \text{ Hz}$ with a Q -value of ≈ 9 . There was a second resonance at 610 Hz with a Q -value $Q \approx 10$. The calibration data for the contact-resonances are listed in Table A5, rows 1–18.

Fall tests

For a second round of experiments, a wooden frame was built that suspended one leg of the landing gear with a polyethylene thread. Fall heights were 3–5 cm; see Fig. A4 and Fig. A5. The thread was cut and the signal emanating from the B&K accelerometer was registered with a digital oscilloscope when it hit the sam-

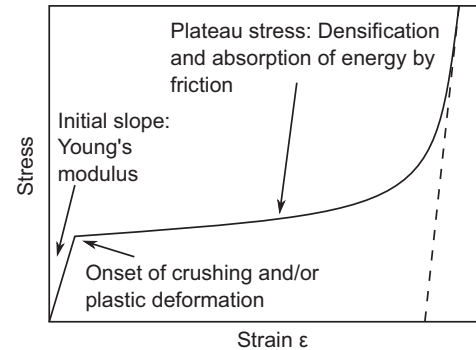


Fig. A6. Stress–strain behavior of a cellular or porous material according to Ashby (2006). If the surface modulus was 3 MPa and its compression strength 3 kPa, the corresponding strain would be $\epsilon \approx 10^{-3}$. Similar behavior has been observed for the KOSI experiments (Thomas et al., 1994).

ple. For a point mass, the fall height on Earth would be 5.1 cm in order to obtain a landing velocity of $v = 1 \text{ m/s}$ like at Agilkia on comet 67P. In our case we used a leg with a foot having a moment of inertia of $T \approx 0.862 \text{ kg/m}^2$ measured from the hinge point and with total mass $m = 1.67 \text{ kg}$. The distances hinge-point to the nylon filament and hinge-point to the center of gravity of the leg were $L_1 = 0.91 \text{ m}$ and 0.631 m , respectively (the moment of inertia is estimated based on the measures and weights of the parts of the leg). Then the required fall height h_{cg} of the center of gravity is given by

$$h_{cg} = T\omega^2 / (2mg), \quad (\text{A6})$$

with an angular velocity $\omega = v/L_1 = 1.09 \text{ s}^{-1}$. This yields $h_{cg} = 3.2 \text{ cm}$ and consequently a fall height of $(0.91/0.631) \times 3.2 = 4.6 \text{ cm}$, about 10% less than the fall height for a point mass.

The results of the fall tests are shown in Table A5 and are plotted in the calibration curve Fig. 9 of the main text. Triangles represent calibration data by fall tests.

A.6. Strain–stress behavior of a cellular material

See Fig. A6.

Table A5

Normalized contact-resonance frequency f_c/f_r ; Young's modulus E and reduced Young's modulus $E_{r,cal}$ for various materials; Rows 1–9: Smooth surfaces. The data were obtained by tapping and are shown in Fig. 9 by squares; Rows 10–18: Porous materials. The data were obtained by tapping and are shown in Fig. 9 by filled circles; Rows 20–29: Various materials. The data were obtained by fall tests and are shown in Fig. 9 by triangles. The parameter p designates the porosity (sample 12 from Mono Lake area, CA, USA and sample 13 from Eifel area, Germany). The density for Aerosil 300 is the so-called bulk density. The properties of this material are described at <http://www.aerosil.com/product/aerosil/en/Pages/default.aspx>.

No.	Material	ρ (10^3 kg/m ³)	E (MPa)	f_c/f_r	$E_{r,cal}$ (MPa)
<i>Results obtained by tapping onto the lid of the sole</i>					
1	Acrylic glass	1.2	4410	4.54	4710
2	Polyamide (red)	1.41	4300	4.54	4940
3	Polyamide (gray)	1.67	5100	4.52	5900
4	Abachi wood: $p=72\%$	0.4	6800	2.28	7000
5	Polystyrene plate	1.05	2310	2.18	2720
6	Polytetrafluorethylene	1.14	4130	3.27	4850
7	Aluminum	2.7	70,000	5.30	79,000
8	Balsawood	0.15	280	1.28	290
9	Polyurethane	1.12	159	0.81	184
10	Polystyrene hard foam	0.016	18	1.12	20
11	Foam	0.027		0.5	10
12	Volcanic stone; $p=75\%$	0.472	778	1.06	969
13	Tuft stone; $p \approx 40\%$	1.1	1341	1.02	1790
14	MSSD (sand)	1.5	469	0.92	530
15	MSSD (sole buried)	1.5	469	1.04	530
16	WF 34 (sand)	1.64	241	1.00	245
17	WF 34 (sole buried)	1.64	241	0.95	245
18	Cork ($\nu=0$)	0.42	30	1.23	30
<i>Results obtained by fall tests</i>					
20	Aerosil 300	0.4		1.03	10
21	Aerosil 300 (sole buried)	0.4		1.11	10
22	Polystyrene hard foam	0.016	18	1.03	20
23	Foam	0.027		0.89	10
24	Polyamide (gray)	1.67	5100	3.86	5900
25	Polytetrafluorethylene	1.14	4130	5.0	4850
26	Balsawood	0.15	280	2.34	290
27	Polyurethane	1.12	159	1.06	184
28	WF34 (sand)	1.64	241	1.17	245
29	Cork ($\nu=0$)	0.42	30	1.27	30

Supplementary materials

Supplementary material associated with this article can be found, in the online version, at [doi:10.1016/j.icarus.2017.09.038](https://doi.org/10.1016/j.icarus.2017.09.038).

References

- Amash, A., Zugenmaier, P., 1997. Thermal and dynamic mechanical investigations of fiber-reinforced polypropylene composites I. J. Appl. Polym. Sci. 63, 11143–11154. doi:[10.1002/\(SICI\)1097-4628\(19970228\)63:9\(1143::AID-APP6\)3.0.CO;2-H](https://doi.org/10.1002/(SICI)1097-4628(19970228)63:9(1143::AID-APP6)3.0.CO;2-H).
- Arnold, W., 2012. Force modulation in atomic force microscopy. In: Bhusan, B. (Ed.), *Encyclopedia of Nanotechnology*. Springer, Berlin, pp. 876–884.
- Arnold, W., Gebhardt, W., Licht, R., Kochan, H., Schieke, S., 2004. Contributions of the Fraunhofer Institute for Non-Destructive Testing to the Rosetta Lander Instrument CASSE: Design, Calibration, Analysis. Saarbrücken, Fraunhofer IZFP, Technisch-Wissenschaftlicher Bericht, Nr. 042011-TW.
- Arnold, W., Möhlmann, D., 2009. Strength of comet material and Hertzian contact-mechanics applied to the landing of philae on comet Churyumov-Gerasimenko. *Aerotech. Missili Spazio: J. Aerospace Sci. Technol. Syst.* 88, 145–149.
- Ashby, M.F., 1983. The mechanical properties of cellular solids. *Metall. Trans. A* 14A, 1755–1769. doi:[10.1007/BF02645546](https://doi.org/10.1007/BF02645546).
- Ashby, M.F., 2006. The properties of foams and lattices. *Phil. Trans. R. Soc. A* 364, 15–30. doi:[10.1098/rsta.2005.1678](https://doi.org/10.1098/rsta.2005.1678).
- Bansemir, H., Haider, O., 1998. Fibre-composites structures for space applications—recent and future developments. *Cryogenics* 38, 51–59. doi:[10.1016/S0011-2275\(97\)00110-0](https://doi.org/10.1016/S0011-2275(97)00110-0).
- Basilevsky, A., Krasil'nikov, S.S., Shiryayev, A.A., Mall, U., Keller, H.U., Skorov, Y.V., Mottola, S., Hviid, S.F., 2016. Estimating the strength of the nucleus material of comet 67P Churyumov-Gerasimenko. *Sol. Syst. Res.* 50, 225–234. doi:[10.1134/S0038094616040018](https://doi.org/10.1134/S0038094616040018).
- Bibring, J.P., Langevin, Y., Carter, J., Eng, P., Gondet, B., Jorda, L., Le Mouélic, S., Mottola, S., Pilorget, C., Poulet, F., Vincendon, M., 2015. 67P/Churyumov-Gerasimenko surface properties, as derived from the first CIVA-P in situ panoramic images. *Science* 349, aab0671-1-3. doi:[10.1126/science.aab0671](https://doi.org/10.1126/science.aab0671).
- Biele, J., Ulamec, S., Maibaum, M., Roll, R., Witte, L., Jurado, E., Munoz, P., Arnold, W., Auster, H.-U., Casas, C., Faber, C., Fantinati, C., Finke, F., Fischer, H.-H., Geurts, K., Guettler, C., Heinisch, P., Herique, A., Hviid, S., Kargl, G., Knapmeyer, M., Knollenberg, J., Kofman, W., Koemle, N., Kühr, E., Lommatsch, V., Mottola, S., de Santayana, R.P., Remeteau, E., Scholten, F., Seidensticker, K.-J., Sierks, H., Spohn, T., 2015. The landing(s) of Philae and inferences about comet surface mechanical properties. *Science* 349, aaa9816. doi:[10.1126/science.aaa9816](https://doi.org/10.1126/science.aaa9816).
- Carneim, T.J., Green, D.J., 2001. Mechanical properties of dry-pressed alumina green bodies. *J. Am. Ceram. Soc.* 84, 1405–1410. doi:[10.1111/j.1151-2916.2001.tb00851.x](https://doi.org/10.1111/j.1151-2916.2001.tb00851.x).
- Dam, C.Q., Brezny, R., Green, D.J., 1990. Compressive behavior and deformation map of an open cell alumina. *J. Mater. Res.* 5, 163–171. doi:[10.1557/JMR.1990.0163](https://doi.org/10.1557/JMR.1990.0163).
- El-Maarry, M.R., Thomas, N., Gracia-Berna, A., Marschall, R., Auger, A.T., Groussin, O., Mottola, S., Pajola, M., Massironi, M., Marchi, S., Hofner, S., Preusker, F., Scholten, F., Jorda, L., Kühr, E., Keller, H.U., Sierks, H., A'Hearn, M.F., Barbieri, C., Barucci, M.A., Bertaux, J.L., Bertini, I., Cremonese, G., Da Deppo, V., Davidsson, B., Debei, S., De Cecco, M., Deller, J., Guttler, C., Fornasier, S., Fulle, M., Gutierrez, P.J., Hofmann, M., Hviid, S.F., Ip, W.H., Knollenberg, J., Koschny, D., Kovacs, G., Kramm, J.R., Kuppers, M., Lamy, P.L., Lara, L.M., Lazzarin, M., Lopez Moreno, J.J., Marzari, F., Michalik, H., Naletto, G., Oklay, N., Pommerol, A., Rickman, H., Rodrigo, R., Tubiana, C., Vincent, J.B., 2015. Fractures on comet 67P/Churyumov-Gerasimenko observed by Rosetta/OSIRIS. *Geophys. Res. Lett.* 42, 5170–5178. doi:[10.1002/2015GL064500](https://doi.org/10.1002/2015GL064500).
- Faber, C., Knapmeyer, M., Roll, R., Chares, B., Schröder, S., Witte, L., Seidensticker, K.J., Fischer, H.-H., Möhlmann, D., Arnold, W., 2015. A method for inverting the touchdown shock of the Philae Lander on Comet 67P/Churyumov-Gerasimenko. *Planet. Space Sci.* 106, 46–55. doi:[10.1016/j.pss.2014.11.023](https://doi.org/10.1016/j.pss.2014.11.023).
- Fellin, W., 2013. Einführung in Eis-, Schnee- und Lawinenmechanik. Springer-Vieweg, Heidelberg doi:[10.1007/978-3-642-25962-3](https://doi.org/10.1007/978-3-642-25962-3).
- Gibson, L.J., Ashby, M.F., 1997. Cellular solids. Cambridge University Press, UK, Cambridge doi:[10.1017/CBO9781139878326](https://doi.org/10.1017/CBO9781139878326).
- Greenberg, J.M., Mizutani, H., Yamamoto, T., 1995. A new derivation of the tensile strength of cometary nuclei: application to comet Shoemaker-Levy 9. *Astronom. Astrophys.* 295, L35–L38.

- Groussin, O., Jorda, L., Auger, A.-T., Kühr, E., Gaskell, R., Capanna, C., Scholten, F., Preusker, F., Lamy, P., Hviid, S., Knollenberg, J., Keller, H.U., Hüttig, C., Sierks, H., Barbieri, C., Rodrigo, R., Koschny, D., Rickman, H., A'Hearn, M.F., Agarwal, J., Barucci, M.A., Bertaux, J.-L., Bertini, I., Boudreault, S., Cremonese, G., Da Deppo, V., Davidsson, B., Debei, S., De Cecco, M., El-Maarry, M.R., Fornasier, S., Fulle, M., Gutiérrez, P.J., Güttler, C., Ip, W.-H., Kramm, J.-R., Küppers, M., Lazzarin, M., Lara, L.M., Lopez Moreno, J.J., Marchi, S., Marzari, F., Massironi, M., Michalik, H., Naletto, G., Oklay, N., Pommerol, A., Pajola, M., Thomas, N., Toth, I., Tubiana, C., Vincent, J.-B., 2015. Gravitational slopes, geomorphology, and material strengths of the nucleus of comet 67P/Churyumov-Gerasimenko from OSIRIS observations. *Astronom. Astrophys.* 583, A32. doi:10.1051/0004-6361/201526379.
- Grün, E., Gebhard, J., Barnun, A., Benkhoff, J., Duren, H., Eich, G., Hische, R., Hübner, W.F., Keller, H.U., Klees, G., Kochan, H., Kolzer, H., Kühr, E., Lämmerzahl, P., Lorenz, E., Markiewicz, W.J., Möhlmann, D., Öhler, A., Scholz, J., Seidensticker, K.J., Rössler, K., Schwehm, G., Steiner, G., Thiel, K., Thomas, H., 1993. Development of a dust mantle on the surface of an insolated ice-dust mixture: results from the KOSI-9 experiment. *J. Geophys. Res.* 98, 15091–15104. doi:10.1029/93JE01134.
- Hatzor, Y.H., Palchick, V., 1997. The influence of grain size and porosity on crack initiation stress and critical flaw length in dolomites. *Int. J. Rock Mech. Mineral Sci.* 34, 805–816. doi:10.1016/S1365-1609(96)00066-6.
- Johnson, K.L., 1985. *Contact mechanics*. Cambridge University Press, Cambridge UK doi:10.1017/CBO9781139171731.
- Kendall, K., McAlford, N., Birchall, J.D., 1987. Elasticity of particle assemblies as a measure of the surface energy of solids. *Proc. Roy. Soc. London.* A412, 269–283. doi:10.1098/rspa.1987.0089.
- Kendall, K., McAlford, N., Birchall, J.D., 1986. *The strength of green bodies*. *Br. Ceram. Proc.* 37, 255–265.
- Knapmeyer, M., Fischer, H.-H., Knollenberg, Seidensticker, K.J., Thiel, K., Arnold, W., Faber, C., Möhlmann, D., 2015. SESAME/CASSE listening to the insertion of the MUPUS PEN at Abydos site, 67P/Churyumov-Gerasimenko. In: *European Planetary Science Congress 2015*, Vol. 10. Vienna, Austria, p. 595.
- Kochan, H., Huebner, W., Sears, D., 1998. Simulation experiments with cometary analog material. *Earth Moon Planets* 80, 369–411. doi:10.1023/A:1006342602452.
- Kochan, H., Roessler, K., Ratke, L., Heyl, M., Hellmann, H., Schwehm, G., 1989. Crustal strength of different model comet materials. In: Hunt, J., Guyenne, T.D. (Eds.), *Int. Workshop on Physics and Mechanics of Cometary Materials*, Vol. SP-302. ESA, Paris, France, Münster, Germany, pp. 115–119.
- Kofman, W., Herique, A., Barbin, Y., Barriot, J.-P., Ciarelli, V., Clifford, S., Edenhofer, P., Elachi, C., Eyraud, C., Goutail, J.-P., Heggy, E., Jorda, L., Lasue, J., Levasseur-Regourd, A.-C., Nielsen, E., Pasquero, P., Preusker, F., Puget, P., Plettemier, D., Rogez, Y., Sierks, H., Statz, C., Svedhem, H., Williams, I., Zine, S., Van Zyl, J., 2015. Properties of the 67P/Churyumov-Gerasimenko interior revealed by CONSERT radar. *Science* 349, aab063. doi:10.1126/science.aab0639.
- Krause, M., 2007. *Untersuchung von Vibrationen an Bord der ESA-Mission mit dem Instrument CASSE*. Master Thesis, Fachhochschule, Aachen, Germany, unpublished.
- Landman, U., Luedtke, W.D., Burnham, N.A., Colton, R.J., 1990. Atomistic mechanism and dynamics of adhesion, nanoindentation, and fracture. *Science* 248, 454–461. doi:10.1126/science.248.4954.454.
- Lange, V.V., 1994. The mechanical impedance analysis method of non-destructive testing: a review. *Nondestruct. Test. Eval.* 11, 177–193. doi:10.1080/10589759408952830.
- Lawn, B., 1993. *Fracture of brittle solids*. Cambridge University Press, Cambridge, UK.
- Leite, M.H., Ferland, F., 2001. Determination of unconfined compressive strength and young's modulus of porous materials by indentation tests. *Eng. Geol.* 59, 267–280. doi:10.1016/S0013-7952(00)00081-8.
- Levitan, E.S., 1960. Forced oscillation of a spin-mass system having combined coulomb and viscous damping. *J. Acoust. Soc. Am.* 32, 1265–1269. doi:10.1121/1.1907893.
- Luding, S., 2008. Cohesive, frictional powders: contact models for tension. *Granular Matter* 10, 235–246. doi:10.1007/s10035-008-0099-x.
- Mansoor-Baghaei, S., Sadegh, A., 2011. Elastic spherical shell impacted with an elastic barrier: a closed form solution. *Int. J. Solids Struct.* 48, 3257–3266. doi:10.1016/j.ijsolstr.2011.07.016.
- Mansoor-Baghaei, S., Sadegh, A.M., 2015. A closed form solution for the impact analysis of elastic ellipsoidal thin shells. *Thin-Walled Struct.* 93, 54–63. doi:10.1016/j.tws.2015.02.021.
- Marinello, F., Passeri, D., Savio, E., 2013. *Acoustic scanning probe microscopy*. Springer, Heidelberg doi:10.1007/978-3-642-27494-7.
- Meisner, T., Wurm, G., Teiser, J., 2012. Experiments on centimeter-sized dust aggregates and their implications for planetesimal formation. *Astron. Astrophys.* 544, A138. doi:10.1051/0004-6361/201219099.
- Mottola, S., Arnold, G., Grothues, H.G., Jaumann, R., Michaelis, H., Neukum, G., Bibring, J.P., Schroder, S.E., Hamm, M., Otto, K.A., Pelivan, I., Proffe, G., Scholten, F., Tirsch, D., Kreslavsky, M., Remeteau, E., Souvannavong, F., Dolives, B., 2015. The structure of the regolith on 67P/Churyumov-Gerasimenko from ROLIS descent imaging. *Science* 349, aab0232. doi:10.1126/science.aab0232.
- Musioliik, G., de Beule, C., Wurm, G., 2017. Analog experiments on tensile strength of dusty and cometary matter. *Icarus* 296, 110–116. doi:10.1017/CBO9781139171731.
- Möhlmann, D., 1996. *Comet 46P/Wirtanen, nucleus reference model*. DLR, Institute for Space Simulation, Cologne.
- Nayak, P.R., 1972. Contact vibrations. *J. Sound Vib.* 22, 297–322. doi:10.1016/0022-460X(72)90168-X.
- Nayfeh, A.H., Mook, D.T., 1995. *Nonlinear oscillations*. John Wiley & Sons, Inc, New York.
- Oliver, W.C., Pharr, G.M., 2004. Measurement of hardness and elastic modulus by instrumented indentation: advances in understanding and refinements to methodology. *J. Mater. Res.* 19, 1–20. doi:10.1557/jmr.2004.0002.
- Pabst, W., Gregorova, E., Ticha, G., 2006. Elasticity of porous ceramics - a critical study of modulus-porosity relations. *J. Eur. Ceram. Soc.* 26, 1085–1097. doi:10.1016/j.jeurceramsoc.2005.01.041.
- Petrovic, J.J., 2003. Review mechanical properties of ice and snow. *J. Mater. Sci.* 38, 1–6. doi:10.1023/A:1021134128038.
- Reissner, E., 1946. On vibrations of shallow spherical shells. *J. Appl. Phys.* 17, 1038–1042. doi:10.1063/1.1707672.
- Roll, R., Witte, L., 2016. ROSETTA lander Philae – touch-down reconstruction. *Planet. Space Sci.* 125, 12–19. doi:10.1016/j.pss.2016.02.005.
- Roll, R., Witte, L., Arnold, W., 2016. ROSETTA Lander Philae – soil strength analysis. *Icarus* 280, 359–365. doi:10.1016/j.icarus.2016.07.004.
- Schieke, S., 2004. *Beiträge zur numerischen Simulation des Instruments CASSE der ESA Rosetta Mission*, PhD thesis, Naturwissenschaftlich-Technische Fakultät III, Saarland University, Saarbrücken, Germany, unpublished.
- Schwartz, M., 1992. *Composite materials handbook*. McGraw-Hill, Inc., New York.
- Seidensticker, K.J., Möhlmann, D., Apathy, I., Schmidt, W., Thiel, K., Arnold, W., Fischer, H.-H., Kretschmer, M., Madlener, D., Peter, A., Trautner, R., Schieke, S., 2007. SESAME - an experiment of the Rosetta Lander Philae: objectives and general design. *Space Sci. Rev.* 128, 301–337. doi:10.1007/s11214-006-9118-6.
- Shokrieh, M.M., Torabizadeh, M.A., Fereidoon, A., 2012. Progressive failure analysis of glass/epoxy composites at low temperatures. *Strength Mater.* 44, 314–324. doi:10.1007/s11223-012-9384-3.
- Skorov, Y., Blum, J., 2012. Dust release and tensile strength of the non-volatile layer of cometary nuclei. *Icarus* 221, 1–11. doi:10.1016/j.icarus.2012.01.012.
- Spohn, T., Knollenberg, J., Ball, A.J., Banaszekiewicz, M., Benkhoff, J., Grott, M., Grygorczuk, J., Hüttig, C., Hagermann, A., Kargl, G., Kaufmann, E., Komle, N., Kühr, E., Kossacki, K.J., Marczewski, W., Pelivan, I., Schrodt, R., Seifert, K., 2015. Thermal and mechanical properties of the near-surface layers of comet 67P/Churyumov-Gerasimenko. *Science* 349, aab0464. doi:10.1126/science.aab0464.
- Tabor, D., 1977. Surface forces and surface interactions. *J. Colloid Interf. Sci.* 58, 2–13. doi:10.1016/0021-9797(77)90366-6.
- Thomas, H., Ratke, L., Kochan, H., 1994. Crushing strength of porous ice-mineral bodies - relevance for comets. *Adv. Space Res.* 14, 207–216. doi:10.1016/0273-1177(94)90271-2.
- Thomas, N., Sierks, H., Barbieri, C., Lamy, P.L., Rodrigo, R., Rickman, H., Koschny, D., Keller, H.U., Agarwal, J., A'Hearn, M.F., Angrilli, F., Auger, A.T., Barucci, M.A., Bertaux, J.L., Bertini, I., Besse, S., Bodewits, D., Cremonese, G., Da Deppo, V., Davidsson, B., De Cecco, M., Debei, S., El-Maarry, M.R., Ferri, F., Fornasier, S., Fulle, M., Giacomini, L., Groussin, O., Gutierrez, P.J., Güttler, C., Hviid, S.F., Ip, W.H., Jorda, L., Knollenberg, J., Kramm, J.R., Kühr, E., Küppers, M., La Forgia, F., Lara, L.M., Lazzarin, M., Moreno, J.J.L., Magrin, S., Marchi, S., Marzari, F., Massironi, M., Michalik, H., Moissl, R., Mottola, S., Naletto, G., Oklay, N., Pajola, M., Pommerol, A., Preusker, F., Sabau, L., Scholten, F., Snodgrass, C., Tubiana, C., Vincent, J.B., Wenzel, K.P., 2015. The morphological diversity of comet 67P/Churyumov-Gerasimenko. *Science* 347, aaa04430. doi:10.1126/science.aaa0440.
- Vidic, M., Harb, S.M., Smith, S.T., 1998. Observations of contact measurements using a resonance-based touch sensor. *Precis. Eng.* 22, 19–36. doi:10.1016/S0141-6359(97)00088-3.
- Young, W.C., Budynas, R.G., 2002. *Roark's formulas for stress and strain*. McGrawHill, New York.
- Yuya, P.A., Hurley, D.C., Turner, J.A., 2008. Contact-resonance atomic force microscopy for viscoelasticity. *J. Appl. Phys.* 104, 074916-1-7. doi:10.1063/1.2996259.